Theory of nonradiative decay dynamics in intensely pumped solid-state laser media via laser photothermal diagnostics

Andreas Mandelis[a] and Joseph Vanniasinkam
Photothermal and Optoelectronic Diagnostics Laboratory, Department of Mechanical Engineering, University of Toronto, Toronto M5S 3G8, Canada

(Received 28 June 1996; accepted for publication 26 August 1996)

A rigorous analytical treatment of nonradiative deexcitation and thermal-conduction transient evolution in solid-state laser media, resulting from intense optical pumping with rectangular pulses from a time-gated laser source, is presented. This situation arises in rate-window photothermal detection from laser rods with bulk and surface absorptions, the latter being due to polishing during the manufacturing of the rod. Numerical simulations of the theory show that the surface nonradiative (optical-to-thermal) energy conversion term is likely to dominate even at absorptances on the order of 1%–2%. Therefore, polishing optimization appears to be necessary in order to minimize laser losses at the surfaces when laser rods are active in a resonator cavity. The present theory also provides physical insights into the very different nature of the bulk- and surface-originating heat-conduction transients, as well as on the profile of the superposition photothermal wave form and its dependence on the optical, thermal, and metastable-state relaxation parameters. As a prelude for input to the photothermal theory, a treatment of the excited-state dynamics of a typical laser manifold pumped by an intense laser beam, away from or near saturation, is developed, and the luminescence and photothermal energy source profiles are calculated analytically. © *1996 American Institute of Physics.* [S0021-8979(96)02723-5]

I. INTRODUCTION

Time-domain photothermal detection has been successfully used to monitor various spectroscopic, metastable-state relaxation, and thermophysical properties of optical (and specifically laser) media in the past 2 decades.[1–3] All existing theoretical treatments of solid-state laser media usually single out one or two particular optical or thermophysical material properties and describe the dynamic evolution of the photothermal signal resulting from probing those properties, e.g., thermal diffusivity,[4,5] optical-absorption coefficient,[6,7] or excited-state lifetime.[1,8] The foregoing specific theoretical models cannot be used with general realistic experimental configurations, where all heat-transport and heat-release-delay-inducing mechanisms are likely to be present simultaneously and operating on similar time scales, as competing degrees of freedom (DOFs) for thermal relaxations. A few theoretical treatments of photothermal effects as related to solid-state laser media have appeared, dealing with the effects of bounding surfaces[7] and of bulk-distributed optical absorption on the thermal profiles.[2,6] With the optical quality of laser materials improving substantially in recent years,[9] photothermal transients from laser-irradiated laser media can be used as powerful diagnostic probes of the optical, thermal, and photonic quality of the medium. Unlike early laser materials, the high-crystal growth quality may no longer be the limiting factor in the optical behavior of manufactured laser rods.[10] The quality of the polish on the bounding surfaces may, indeed, limit the performance of otherwise nearly perfect rods in a laser cavity, by lowering the effective figure of merit. As a direct consequence, surface-layer-generated photothermal signals may possibly dominate bulk heat release and evolution, thus becoming very sensitive nondestructive probes of the nonradiative (optical-to-thermal) energy conversion processes occurring at the crystal surface. Specifically, in recent frequency-domain photothermal studies of Ti^{3+}:Al_2O_3 crystal rods it has been found that the nonzero absorptance of the surface polish (i.e., damage) layers constitutes an additional heat source.[11] The transient effects of this surface source must be taken into consideration, especially in assessing its relative contribution with respect to bulk optical heating. Time-domain photothermal experiments using pulsed, or time-gated, laser sources must be used in order to deconvolute bulk and surface thermal generation from the different temporal evolution profiles of these two nonradiative deexcitation processes. Frequency-scanned photothermal detection is another available method with higher signal-to-noise ratio (SNR) than time-domain detection; nevertheless the complicated time multiplexing of each frequency component makes it, in our experience, difficult to give accurate diagnosis of the origin(s) and/or relative contribution(s) of surface and bulk components to the amplitude and phase of the photothermal signal. Recently, we have combined the high SNR of frequency-domain lock-in detection methods with the more straightforward temporal-delay/evolution time-domain interpretations, in introducing a novel photothermal rate-window (RW) technique.[3] RW photothermal detection requires repetitive square-pulse optical excitation and lock-in monitoring of the fundamental Fourier coefficient of the sample response under pulse-duration (τ_p) or pulse-repetition (T_0) scan. Therefore, the temporal evolution of a photothermal transient generated by a time-gated incident optical pulse, which is absorbed partly on the surface and partly in the bulk, is required. Santos and Miranda[2] described the photothermal transient response to a square laser pulse of an absorbing surface layer

[a]Electronic mail: mandelis@me.utoronto.ca

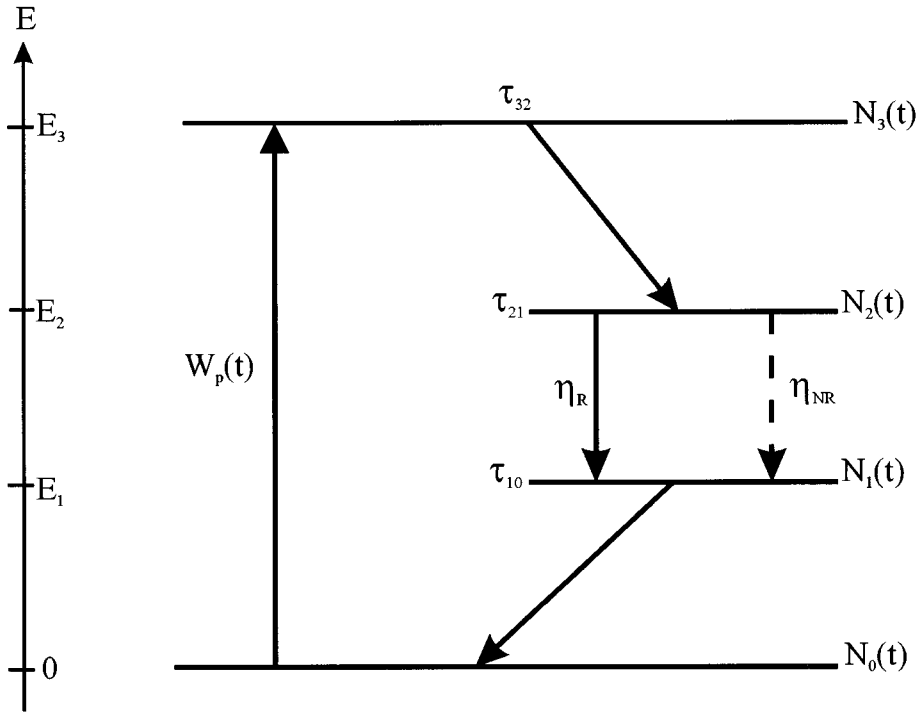

FIG. 1. Typical energy diagram of a four-level laser system. $N_j(t)$: population of level $|j\rangle$; τ_{jk}: total lifetime of level $|j\rangle$ undergoing transition to level $|k\rangle$; η_R (η_{NR}): radiative (nonradiative) quantum yield of metastable level $|2\rangle$; $W_p(t)$: ground-state pumping rate.

in an optically transparent solid, using a one-dimensional model. Unfortunately, this theoretical transient behavior can be severely perturbed by actual experimental configurations, such as the nonzero excited-state spontaneous lifetime, the finite spot-size of the pump laser beam, and the finite thermal transfer time from solid to gas. Bechtel[6] has addressed bulk or surface photothermal transient behavior through the low or high value of the optical-absorption coefficient, respectively. Unfortunately, his theory cannot be used for a comparative study of simultaneous surface and bulk photothermal sources. Furthermore, the effectively adiabatic boundary condition he used for the laser-irradiated surface turns out to be too restrictive toward the interpretation of our (preliminary) results from Ti^{3+}:Al_2O_3 laser rods, while his theory also ignores time delays due to the deexcitation of metastable states and laser-medium saturation resulting from intense pumping.

In this work, the photothermal response of a solid-state laser medium excited by an optical pulse of finite duration τ_p is modeled rigorously. Section II deals with the generalized deexcitation dynamics of the excited-state manifold typical of an intensely optically pumped laser medium in the presence of optical saturation. The optical transient of the metastable-level population is derived, its evolution being proportional to the luminescence signal. Furthermore, using the excited-state temporal profile as the source of nonradiative relaxations from the metastable level, the bulk thermal-rate density function is derived, leading to the bulk thermal (nonradiative) relaxation transient. Section III develops the transient heat conduction Green's function formalism for a semi-infinite geometry of the laser medium: It includes the delayed bulk thermal source due to the nonzero metastable-state relaxation time (and the concomitant nonradiative quantum yield), as well as a surface absorptance source leading to a purely surface-layer nonradiative relaxation. Section IV reduces the general formalism to a few important special cases, directly comparable to existing theoretical expressions. Section V gives numerical simulations of the superposition transient photothermal signal, with emphasis on the relative contributions from the bulk and the surface absorptions. Section VI summarizes the conclusions of the theory.

II. OPTICAL- AND THERMAL-DECAY CHANNELS OF DEEXCITATION DYNAMICS IN INTENSELY PUMPED LINEAR LASER MEDIA

The deexcitation dynamics of a general, four-level laser medium is now considered under intense ground-state pumping conditions. In this case, the usual assumption of constant ground-state population[12] is not valid. Intense pumping of laser materials is often required with photothermal detection by infrared radiometry[8] owing to the low signal levels and low SNRs obtained with this technique. Of course, the main advantage of infrared photothermal radiometry is its entirely remote, noncontacting nature, along with the availability of fast ($\geqslant$1 MHz) photovoltaic and photoconductive blackbody detectors. Figure 1 shows a typical four-level laser energy diagram. The medium is pumped by an optical source up to level $|3\rangle$ with pumping rate $W_p(t)$. The optical pumping is assumed to be intense enough to create a measurably time-dependent ground-state population reaching the saturation threshold of the laser medium under consideration but not driving nonlinear absorption processes. The instantaneous ($\sim$ps) upper-level decay is assumed to be entirely nonradia-

tive. The deexcitation of the metastable level $|2\rangle$ is assumed, however, to occur via radiative and nonradiative pathways with quantum yields η_R and $\eta_{\rm NR}=1-\eta_R$, respectively. The relevant rate equation for level $|3\rangle$ is

$$\frac{dN_3(t)}{dt}=W_p(t)N_0(t)-\frac{1}{\tau_{32}}N_3(t). \tag{1}$$

Assuming $N_3(0)=0$, and further assuming that $\tau_{32}\ll t_{\rm min}$, where $t_{\rm min}$ is the earliest observation time, so that $dN_3(t)/dt=0$ on the time scale of the photothermal experiment, Eq. (1) results in a simple expression,

$$N_3(t)\simeq\tau_{32}W_p(t)N_0(t). \tag{2}$$

Similarly, the rate equation for level $|2\rangle$ can be put in the following form, in view of Eq. (2):

$$\frac{dN_2(t)}{dt}=\frac{1}{\tau_{32}}N_3(t)-\frac{1}{\tau_{21}}N_2(t)\simeq W_p(t)N_0(t)-\frac{1}{\tau_{21}}N_2(t). \tag{3}$$

Here it is assumed that optical excitation occurs outside a laser cavity for diagnostic purposes of the optical quality of the rod material, and thus no stimulated component is included in the rate equations. Treating the deexcitation of level $|1\rangle$ in a manner similar to that of $|3\rangle$, i.e., assuming $\tau_{10}\ll t_{\rm min}$, the rate equation yields

$$N_1(t)\simeq(\tau_{10}/\tau_{21})N_2(t)\simeq 0, \tag{4}$$

provided that $\tau_{10}\ll\tau_{21}$, a commonly satisfied condition with solid-state laser media. Finally, owing to the fact that the total laser-active population N_T is conserved (i.e., constant in time), one may write

$$\sum_{j=0}^{3}N_j(t)=N_T \tag{5a}$$

or

$$\sum_{j=0}^{3}\left(\frac{dN_j(t)}{dt}\right)=0. \tag{5b}$$

Solving Eq. (5a) for $N_0(t)$, inserting in Eq. (3) and taking the low occupation of levels $|3\rangle$ and $|1\rangle$ into account, $N_1(t)$, $N_3(t)\ll N_T\simeq N_0(t)+N_2(t)$, gives

$$\frac{dN_2(t)}{dt}+[W_p(t)+\tau_{21}^{-1}]N_2(t)\simeq W_p(t)N_T. \tag{6}$$

This equation can be solved once the $W_p(t)$ functional dependence on time is known. For a simple rectangular optical pulse (experimentally the acousto-optically time-gated output of a cw laser used in photothermal RW detection[3]),

$$W_p(t)=\begin{cases}W_{p0}, & t<\tau_p,\\ 0, & t>\tau_p.\end{cases} \tag{7}$$

Equation (6) has the solution

$$N_2(t)=W_{p0}N_T\tau\begin{cases}1-e^{-t/\tau}, & t\leqslant\tau_p,\\ (e^{\tau_p/\tau_{21}}-e^{-W_{p0}\tau_p})e^{-t/\tau_{21}}, & t\geqslant\tau_p,\end{cases} \tag{8}$$

where

$$\frac{1}{\tau}\equiv\frac{1}{\tau_{21}}+W_{p0}. \tag{9}$$

$N_2(t)$ in Eq. (8) further describes the temporal behavior of the luminescence signal from a laser medium, since the radiative emission rate is proportional to the population of the metastable state and to the radiative quantum yield, $\eta_R=\tau/\tau_{21}$.

In most laser media, a finite nonradiative quantum yield $\eta_{\rm NR}$ is present along with η_R.[12] In Ti sapphire in particular, the optical-to-thermal energy conversion process involves deexcitation to the electronic ground state via the strong lattice-phonon system coupling.[13] Therefore, the temperature rise distribution at the onset of nonradiative relaxation reflects the spatial distribution of active ions, which are stationary in the host crystal. As a consequence, there is no electronic transport involved, as is the case with the nonradiative decay in semiconductors. Based on the energy diagram of Fig. 1, the release of the thermal energy density $Q(t)$ in an optically excited four-level medium is given by

$$\frac{dQ(t)}{dt}=\frac{E_{32}}{\tau_{32}}N_3(t)+\eta_{\rm NR}\left(\frac{E_{21}}{\tau_{21}}\right)N_2(t)+\left(\frac{E_{10}}{\tau_{10}}\right)N_1(t)\quad({\rm W/m^3}), \tag{10a}$$

where

$$E_{ij}\equiv E_i-E_j. \tag{10b}$$

Taking the low occupation of levels $|3\rangle$ and $|1\rangle$ into account, Eq. (10) can be written using Eq. (2),

$$\frac{dQ(t)}{dt}=N_TE_{32}W_p(t)+\left(\frac{E_{20}^{\rm NR}}{\tau_{21}}-E_{32}W_p(t)\right)N_2(t), \tag{11}$$

where

$$E_{20}^{\rm NR}\equiv\eta_{\rm NR}E_{21}+E_{10} \tag{12}$$

is the portion of the energy deposited at the metastable level $|2\rangle$, which is released as thermal energy, i.e., nonradiatively. In Eq. (11), the pumping rate $W_p(t)$ can also be written in terms of the incident optical intensity $I_o(t)$ and the absorption cross section $\sigma_{30}(\lambda)$ of the laser medium,

$$W_p(t)=\left(\frac{\sigma_{30}(\lambda)}{E_{30}}\right)I_o(t). \tag{13}$$

In the presence of intense pumping, the optical absorption coefficient β_{30} corresponding to the absorption cross section σ_{30} becomes time dependent, as the populations of the states $|0\rangle$ and $|2\rangle$ vary significantly. The rate equation governing the population $N_2(t)$ is given by Eq. (3). Using $N_T\simeq N_0(t)+N_2(t)$ easily yields a corresponding rate equation for $N_0(t)$. Defining the population difference between $|0\rangle$ and $|2\rangle$ by

$$\Delta N(t)\equiv N_0(t)-N_2(t) \tag{14}$$

results in the following rate equation for ΔN:

$$\frac{d}{dt}\Delta N(t)+[W_p(t)+\tau_{21}^{-1}]\Delta N(t)=[\tau_{21}^{-1}-W_p(t)]N_T. \tag{15}$$

The solution of this equation with the rectangular pulse dependence of Eq. (7) for $W_p(t)$ is

$$\Delta N(t)=N_T\begin{cases}\tau[(\tau_{21}^{-1}-W_{p0})+2W_{p0}\ \exp(-t/\tau)], & t\leqslant\tau_p,\\ 1-2W_{p0}\tau(1-e^{-\tau_p/\tau})\exp\left[-\left(\dfrac{t-\tau_p}{\tau_{21}}\right)\right], & t\geqslant\tau_p.\end{cases}\tag{16}$$

Finally, using the defining relationship between β_{30} and σ_{30},[12]

$$\beta_{30}(t;\lambda)=\sigma_{30}(\lambda)\Delta N(t)\equiv\beta_m[\Delta N(t)/N_T]\tag{17}$$

gives an expression for the time-dependent optical-absorption coefficient under saturation conditions,

$$\beta_{30}(t;\lambda)=\beta_m(\lambda)\begin{cases}\tau[(\tau_{21}^{-1}-W_{p0})+2W_{p0}e^{-t/\tau}], & t\leqslant\tau_p,\\ 1-2W_{p0}\tau(e^{\tau_p/\tau_{21}}-e^{-W_{p0}\tau_p})e^{-t/\tau_{21}}, & t\geqslant\tau_p,\end{cases}\tag{18}$$

where $\beta_m(\lambda)$ is the maximum possible value of β_{30} under completely unsaturated conditions: $\beta_m=\sigma_{30}N_T$. For the rectangular optical pulse profile of Eq. (7), $N_2(t)$ is given by Eq. (8). In this case, Eq. (11) becomes

$$\frac{dQ(t)}{dt}=\frac{W_{p0}N_T}{1+W_{p0}\tau_{21}}\begin{cases}E_{30}^{\rm NR}(1+be^{-t/\tau}), & t<\tau_p,\\ E_{20}^{\rm NR}(e^{\tau_p/\tau_{21}}-e^{-W_{p0}\tau_p})e^{-t/\tau_{21}}, & t>\tau_p,\end{cases}\tag{19}$$

where

$$E_{30}^{\rm NR}\equiv E_{32}+\eta_{\rm NR}E_{21}+E_{10}\tag{20}$$

in analogy with Eq. (12). Also,

$$b\equiv(\tau_{21}W_{p0}E_{32}-E_{20}^{\rm NR})/E_{30}^{\rm NR},\tag{21}$$

representing the fraction of the total thermal energy $E_{30}^{\rm NR}$ contributed by the population in level $|2\rangle$ upon time-delayed deexcitation into the ground state $|0\rangle$. Inspection of Eq. (19) shows a discontinuous drop in the heat-density release rate at $t=\tau_p$ of magnitude $E_{32}(1+\tau_{21}W_{p0}e^{-\tau_p/\tau})$. This is due to the (assumed) instantaneous deexcitation of the population in level $|3\rangle$ down to level $|2\rangle$, following the switching off of the optical pump. Figure 2 shows a family of $dQ(t)/dt$ profiles for various pumping rates W_{p0}, corresponding to the Ti^{3+}:Al_2O_3 system.[14] The value $\eta_{\rm NR}=0.10$ was obtained using photopyroelectric detection at $\lambda=490$ nm,[15] for optical excitation and nonradiative decay of a rod with figure of merit FOM=800. The total thermal energy density released in the laser medium within the duration τ_p of the pulse of intensity I_o is

$$Q(\tau_p)=I_o\tau_p(E_{30}^{\rm NR}/E_{30}).\tag{22}$$

III. TRANSIENT HEAT CONDUCTION: GREEN'S FUNCTION APPROACH

Assume a semi-infinite cylindrical laser medium, both laterally (radially) and lengthwise, corresponding to a thick and long laser rod. The effects of the existence of boundary surfaces for finite radii can be modeled as described elsewhere.[7] A pump laser beam is incident on the (polished) surface of the medium, with intensity profile

$$I(r)=\frac{2P_o}{\pi R^2}\,e^{-2r^2/R^2}\quad(\mathrm{W/m^2})\tag{23}$$

where P_o is the incident optical power (W), r is the radial coordinate, Fig. 3, and R is the beam waist. It is most convenient to describe the spatial and temporal evolution of the photothermal field in the laser medium by means of the cylindrical coordinate Green's function for the given geometry,

$$\frac{1}{r}\frac{\partial}{\partial r}\left(r\,\frac{\partial G}{\partial r}\right)+\frac{\partial^2 G}{\partial z^2}-\frac{1}{\alpha}\frac{\partial G}{\partial t}=-\frac{1}{2\pi k r_0}\,\delta(r-r_0)\,\delta(z-z_0)\,\delta(t-t_0),\qquad 0\leqslant r<\infty,\ \ z\geqslant 0,\tag{24}$$

where α (k) is the thermal diffusivity (conductivity), and (r,z,t), (r_0,z_0,t_0) are the observation and source coordinates, respectively. The translated photothermal field function in the medium,

$$\theta(r,z,t)\equiv T(r,z,t)-T_\infty,\tag{25}$$

where T_∞ is the ambient temperature and satisfies the following equation:

$$\frac{1}{r}\frac{\partial}{\partial r}\left(r\,\frac{\partial\theta}{\partial r}\right)+\frac{\partial^2\theta}{\partial z^2}-\frac{1}{\alpha}\frac{\partial\theta}{\partial t}=-\frac{1}{k}\,\rho(r,z,t),\tag{26a}$$

subject to the initial and boundary conditions

$$\theta(r,z,0)=0,\tag{26b}$$

$$\theta(\infty,z,t)=0,\tag{26c}$$

$$\theta(r,\infty,t)=0,\tag{26d}$$

$$k\,\frac{\partial}{\partial z}\,\theta(r,z,t)\bigg|_{z=0}=h\,\theta(r,0,t). \tag{26e}$$

Here $\rho(r,z,t)$ is the laser medium volume thermal source, and h is the heat transfer coefficient for boundary conditions of the third kind.[16] Specifically for infrared photothermal radiometric detection, the nonlinear contribution due to the $\sigma[T^4(r,0,t)-T_\infty^4]$ dependence (assuming semi-infinite detection bandwidth) must formally be taken into account in Eq. (26e).[16] Bechtel[6] has argued that this contribution is negligible when large pump laser irradiances are involved, owing to the small value of the Stefan–Boltzmann constant $\sigma=5.67\times10^{-8}$ W/m^2 K.[4] The present theoretical treatment is consistent with Bechtel's argument, in order to avoid the obvious complexities of nonlinear conduction heat transfer.[17] The observed linearity of our (preliminary) experimental photothermal signals with incident laser power level on Ti:sapphire laser rods further attests to the validity of the linear approximation, Eq. (26e). In view of Eqs. (26b)–(26e), the Green's function must satisfy similar homogeneous initial condition (26b) and homogeneous boundary conditions (26c) and (26d). Separating G into the product of a radial and an axial function

$$\begin{aligned}&G(r,z,t|r_0,z_0,t_0)\\&\quad=G_R(r,t|r_0,t_0)G_A(z,t|z_0,t_0)\end{aligned} \tag{27}$$

results in two expressions: For the radial function which satisfies

$$G_R(r,t|r_0,0)=G_R(r,t|\infty,t_0)=0,$$

Ref. 18, Eq. (7.3), p. 202, gives

$$\begin{aligned}G_R(r,t|r_0,t_0)=&\frac{1}{4\pi\alpha(t-t_0)}\exp\left(-\frac{(r^2+r_0^2)}{4\alpha(t-t_0)}\right)\\&\times I_0\left(\frac{rr_0}{2\alpha(t-t_0)}\right),\end{aligned} \tag{28}$$

where $I_0(x)$ is the modified Bessel function of the first kind of order zero. For the axial function which satisfies

$$G_A(z,t|\infty,t_0)=G_A(z,t|z_0,0)=0$$

and

$$k\,\frac{\partial}{\partial z_0}\,G_A(z,t|z_0,t_0)|_{z_0=0}=hG_A(z,t|0,t_0),$$

Ref. 18, Eq. (X30.1), p. 499, gives an expression which after a modification becomes

$$\begin{aligned}&G_A(z,t|z_0,t_0)\\&=\frac{1}{\sqrt{4\pi\alpha(t-t_0)}}\left[\exp\left(-\frac{(z-z_0)^2}{4\alpha(t-t_0)}\right)\right.\\&\quad\left.+\exp\left(-\frac{(z+z_0)^2}{4\alpha(t-t_0)}\right)\right]-\frac{1}{\sqrt{\alpha\tau_h}}\\&\quad\times\exp\left(-\frac{(z+z_0)^2}{4\alpha(t-t_0)}\right)Y\left[\frac{z+z_0}{\sqrt{4\alpha(t-t_0)}}+\left(\frac{t-t_0}{\tau_h}\right)^{1/2}\right],\end{aligned} \tag{29}$$

where

$$Y(z)\equiv e^{z^2}\,\mathrm{erfc}(z) \tag{30}$$

and τ_h is the characteristic thermal transfer time from the surface of the laser medium into the surrounding gas (air),

$$\tau_h\equiv\frac{k^2}{h^2\alpha}. \tag{31}$$

The translated temperature field in the medium is given in terms of well-known integrals of Green's function,[16,18]

$$\begin{aligned}\theta(r,z)=\frac{\alpha}{k}\Bigg(&\int_0^t dt_0\int_{V_0}\int\int G(r,z,t|r_0,z_0,t_0)\\&\times\rho(r_0,z_0,t_0)dV_0+\int_0^t dt_0\int_{S_0}\int G(r,z,t|r_0,0,t_0)\\&\times Q_0(r_0,t_0)dS_0\Bigg).\end{aligned} \tag{32}$$

Here V_0 is the source volume and S_0 is the bounding surface (i.e., the plane $z_0=0$). Q_0 is the field-determining surface source. Performing the angular integrations in cylindrical coordinates, and using Eq. (28), results in the following expression:

$$\begin{aligned}\frac{k}{2\pi\alpha}\,\theta(r,z,t)=&\int_0^t dt_0\int_0^\infty G_R(r,t,|r_0,t_0)r_0\,dr_0\\&\times\int_0^\infty G_A(z,t|z_0,t_0)\rho(r_0,z_0,t_0)dz_0\\&+\int_0^t G_A(z,t|0,t_0)dt_0\int_0^\infty G_R(r,t|r_0,t_0)\\&\times Q_0(r_0,t_0)r_0\,dr_0.\end{aligned} \tag{33}$$

The bulk (volume) thermal source ρ can be determined from

(i) the net optical power density which is transmitted past the surface layer of absorptance $\Gamma_s(\lambda)$;
(ii) the optical-absorption profile in the laser medium, including saturation phenomena and assumed to be homogeneous and obeying the Beer–Lambert law;
(iii) the incident pump-beam spatial profile in the radial coordinate, Eq. (23); and
(iv) the heat-release rate density of Eq. (19).

Therefore, in the source coordinates

$$\rho(r_0,z_0,t_0)=(1-\Gamma_s)e^{-2r_0^2/R^2}e^{-\beta_{30}(t)z_0}F(t_0), \tag{34a}$$

where

$$F(t_0)\equiv\frac{2P_o\beta_{30}(t_0)}{\pi R^2E_{30}(1+W_{p0}\tau_{21})}$$

$$\times\begin{cases} E_{30}^{\mathrm{NR}}(1+be^{-t_0/\tau}), & t_0<\tau_p, \\ E_{20}^{\mathrm{NR}}(e^{\tau_p/\tau_{21}}-e^{-W_{p0}\tau_p})e^{-t_0/\tau_{21}}, & t_0>\tau_p \end{cases}. \tag{34b}$$

The surface thermal source $Q_0(r_0,t_0)$ is the result of optical absorption within the virtual surface layer of absorptance $\Gamma_s(\lambda)$ and (the assumed) 100% optical-to-thermal energy conversion efficiency in this layer. The surface nonradiative quantum efficiency $\eta_{\mathrm{NR}}^{(s)}=1$ assumed here is consistent with our earlier findings[9,11] in Ti:sapphire laser rods with polished surfaces. This value appears physically reasonable as the result of some degree of damage to the crystal incurred during the polishing process. Therefore, in the source coordinates

$$Q_0(r_0,t_0)=\Gamma_s(\lambda)e^{-2r_0^2/R^2}q_0(t_0), \tag{35}$$

where

$$q_0(t_0)\equiv\frac{2P_o}{\pi R^2}\begin{cases} 1, & t_0<\tau_p, \\ 0, & t_0>\tau_p. \end{cases} \tag{36}$$

Insertion of Eqs. (34)–(36) in Eq. (33) yields in compact form

$$\frac{k}{2\pi\alpha}\,\theta(r,0,t)=(1-\Gamma_s)\int_0^t F(t_0)K(r,t;t_0)H(t;t_0)dt_0$$

$$(\text{volume contribution})$$

$$+\Gamma_s\int_0^t q_0(t_0)K(r;t;t_0)G_A(0,t|0,t_0)dt_0$$

$$(\text{surface contribution}), \tag{37}$$

where the following integrals have been defined:

$$K(r,t;t_0)\equiv\int_0^\infty G_R(r,t|r_0,t_0)e^{-2r_0^2/R^2}r_0\,dr_0 \tag{38}$$

and

$$H(t;t_0)\equiv\int_0^\infty G_A(0,t|z_0,t_0)e^{-\beta_{30}(t_0)z_0}\,dz_0. \tag{39}$$

Appendix A shows the details of the calculation of K and H in terms of tabulated functions. Inserting Eqs. (A3) and (A10) in Eq. (37) results in the desired photothermal field function,

$$\theta(r,0,t)=\frac{\alpha R^2}{k}\left\{\frac{\Gamma_s}{\sqrt{\alpha}}\left[\frac{1}{\sqrt{\pi}}\int_0^t\frac{q_0(t_0)}{[8\alpha(t-t_0)+R^2]\sqrt{t-t_0}}\exp\left(-\frac{2r^2}{8\alpha(t-t_0)+R^2}\right)dt_0\right.\right.$$
$$-\frac{1}{\sqrt{\tau_h}}\int_0^t\left(\frac{q_0(t_0)Y[\sqrt{(t-t_0)/\tau_h}]}{8\alpha(t-t_0)+R^2}\right)\exp\left(-\frac{2r^2}{8\alpha(t-t_0)+R^2}\right)dt_0\Bigg]+(1-\Gamma_s)$$
$$\times\left(\int_0^t\frac{F(t_0)Y[\sqrt{(t-t_0)/\tau_\beta(t_0)}]\exp\{-2r^2/[8\alpha(t-t_0)+R^2]\}dt_0}{[1-\sqrt{\tau_h/\tau_\beta(t)}][8\alpha(t-t_0)+R^2]}\right.$$
$$\left.\left.-\sqrt{\tau_h}\int_0^t\frac{F(t_0)Y[\sqrt{(t-t_0)/\tau_\beta(t_0)}]\exp\{-2r^2/[8\alpha(t-t_0)+R^2]\}dt_0}{[\sqrt{\tau_\beta(t_0)}-\sqrt{\tau_h}][8\alpha(t-t_0)+R^2]}\right)\right\}. \tag{40}$$

For many photothermal experimental systems, a signal proportional to the temperature evolution at the center of the photoexcited medium surface, $r=0$, is obtained (e.g., with thermoreflectance detection using a tightly focused probe laser beam,[19] or with infrared photothermal radiometry using a narrow-aperture HgCdTe detector[8]). For these types of geometries, the following simplified expressions can be obtained from Eqs. (34), (36), and (40):

$$\theta(0,0,t)\equiv\theta_{\mathrm{s(urface)}}(0,0,t)+\theta_{\mathrm{b(ulk)}}(0,0,t), \tag{41a}$$

with

$$\theta_s(0,0,t)=\frac{R^2\alpha}{k\sqrt{\pi}}\,\Gamma_s\left[\int_0^t q_0(t_0)\,\frac{dt_0}{[8\alpha(t-t_0)+R^2]\sqrt{t-t_0}}\right.$$
$$\left.-\left(\frac{\pi}{\tau_h}\right)^{1/2}\int_0^t q_0(t_0)\left(\frac{Y[\sqrt{(t-t_0)/\tau_h}]}{8\alpha(t-t_0)+R^2}\right)dt_0\right] \tag{41b}$$

and

$$\theta_b(0,0,t)=\frac{R^2\alpha(1-\Gamma_s)}{k}$$
$$\times\left(\int_0^t\frac{F(t_0)Y[\sqrt{(t-t_0)/\tau_h}]dt_0}{[1-\sqrt{\tau_h/\tau_\beta(t_0)}][8\alpha(t-t_0)+R^2]}\right.$$
$$\left.-\sqrt{\tau_h}\int_0^t\frac{F(t_0)Y[\sqrt{(t-t_0)/\tau_\beta(t_0)}]dt_0}{[\sqrt{\tau_\beta(t_0)}-\sqrt{\tau_h}][8\alpha(t-t_0)+R^2]}\right). \tag{41c}$$

Explicit expressions during and after the pulse duration τ_p can be written upon consideration of the time dependences of the sources $q_0(t_0)$ and $F(t_0)$,

$$\theta_s(0,0,t\leq\tau_p)=\frac{2P_o\sqrt{\alpha}\Gamma_s}{\pi^{3/2}k}\left[\frac{1}{\sqrt{2\alpha}R}\tan^{-1}\left(\frac{\sqrt{8\alpha t}}{R}\right)\right.$$

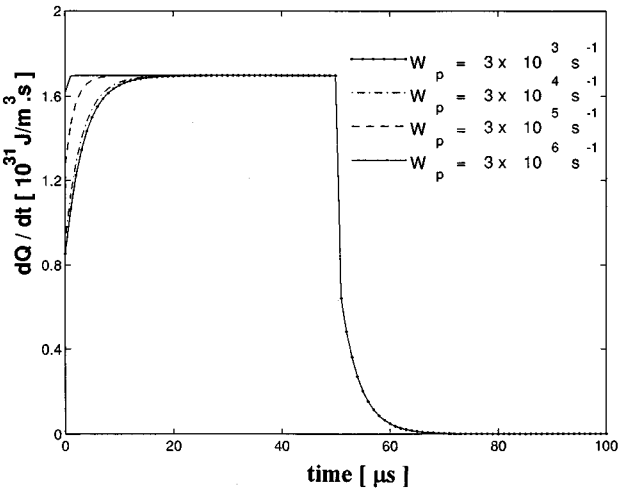

FIG. 2. Decay rate profiles of deexcitation thermal densities $dQ(t)/dt$ in Ti: sapphire corresponding to various strong unsaturated pumping rates W_p and $\tau_p=50$ μs; $E_{30}=19\,455$ cm^{-1}; $E_{32}=3239$ cm^{-1}; $E_{21}=14\,380$ cm^{-1}; $E_{10}=1836$ cm^{-1} (Ref. 20). Also: $\tau_{21}=3.5$ μs; $\eta_{\rm NR}=0.1$ corresponding to $\lambda=490$ nm as measured photopyroelectrically (Ref. 11).

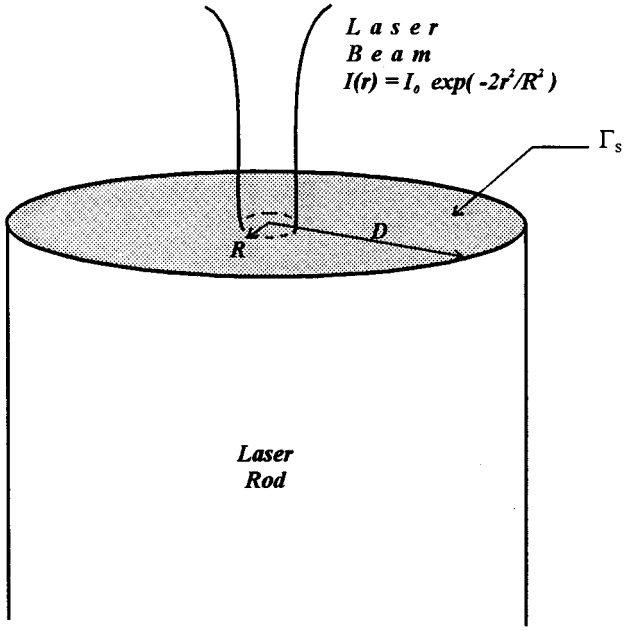

FIG. 3. Geometry of optically pumped laser rod of radial dimension $D\gg R$ (R: pump-beam waist). The polished surface absorptance is Γ_s. The rod length is much longer than all characteristic photothermal length parameters in the (mathematically semi-infinite) medium.

$$-\left(\frac{\pi}{\tau_h}\right)^{1/2}\int_0^t \frac{Y[\sqrt{(t-t_0)/\tau_h}]}{8\alpha(t-t_0)+R^2}\,dt_0\Bigg] \tag{42a}$$

and

$$\theta_b(0,0,t\leqslant\tau_p) = \frac{2P_o\sqrt{\alpha}(1-\Gamma_s)(E_{30}^{\rm NR}/E_{30})}{\pi k(1+W_{p0}\tau_{21})} \times\left(\int_0^t \frac{Y[\sqrt{(t-t_0)/\tau_h}](1+be^{-t_0/\tau})dt_0}{[\sqrt{\tau_\beta(t_0)}-\sqrt{\tau_h}][8\alpha(t-t_0)+R^2]} - \sqrt{\tau_h}\int_0^t \frac{Y[\sqrt{(t-t_0)/\tau_\beta(t_0)}](1+be^{-t_0/\tau})dt_0}{[\tau_\beta(t_0)-\sqrt{\tau_h\tau_\beta(t_0)}][8\alpha(t-t_0)+R^2]}\right). \tag{42b}$$

Also,

$$\theta_s(0,0,t\geqslant\tau_p)=\frac{2P_o\sqrt{\alpha}\Gamma_s}{\pi^{3/2}k}\left[\frac{1}{\sqrt{2\alpha}R}\tan^{-1}\left(\frac{\sqrt{8\alpha\tau_p}}{R}\right) -\left(\frac{\pi}{\tau_h}\right)^{1/2}\int_0^{\tau_p}\frac{Y[\sqrt{(t-t_0)/\tau_h}]}{8\alpha(t-t_0)+R^2}\,dt_0\right] \tag{43a}$$

and

$$\theta_b(0,0,t\geqslant\tau_p)=\frac{2P_o\sqrt{\alpha}(1-\Gamma_s)}{\pi k(1+W_{p0}\tau_{21})}\left[\frac{E_{30}^{\rm NR}}{E_{30}}\left(\int_0^{\tau_p}\frac{Y[\sqrt{(t-t_0)/\tau_h}](1+be^{-t_0/\tau})dt_0}{[\sqrt{\tau_\beta(t_0)}-\sqrt{\tau_h}][8\alpha(t-t_0)+R^2]} - \sqrt{\tau_h}\int_0^{\tau_p}\frac{Y[\sqrt{(t-t_0)/\tau_\beta(t_0)}](1+be^{-t_0/\tau})dt_0}{[\tau_\beta(t_0)-\sqrt{\tau_h\tau_\beta(t_0)}][8\alpha(t-t_0)+R^2]}\right) +\left(\frac{E_{20}^{\rm NR}}{E_{30}}\right)(e^{\tau_p/\tau_{21}}-e^{W_{p0}\tau_{21}})\left(\int_{\tau_p}^t\frac{Y[\sqrt{(t-t_0)/\tau_h}]e^{-t_0/\tau_{21}}\,dt_0}{[\sqrt{\tau_\beta(t_0)}-\sqrt{\tau_h}][8\alpha(t-t_0)+R^2]} - \sqrt{\tau_h}\int_{\tau_p}^t\frac{Y[\sqrt{(t-t_0)/\tau_\beta(t_0)}]e^{-t_0/\tau_{21}}\,dt_0}{[\tau_\beta(t_0)-\sqrt{\tau_h\tau_\beta(t_0)}][8\alpha(t-t_0)+R^2]}\right)\right]. \tag{43b}$$

It is easy to verify that the given expressions are continuous at the instant $t=\tau_p$ (end of pulse), provided that the appropriate terms for $\beta_{30}(t)$ and $\tau_\beta(t)$ are used from Eq. (18) corresponding to $t\leqslant\tau_p$ or $t\geqslant\tau_p$ as implied by the limits of the foregoing integrals.

IV. SPECIAL CASES OF $\theta(0,0,t)$

The foregoing three-dimensional treatment can be easily reduced to a one-dimensional theory by setting the pump laser-beam size infinite. This may be achieved experimentally and theoretically in the limit

$$R^2\gg 8\alpha(t-t_0). \tag{44}$$

As long as the observation time is restricted within the time scale indicated by inequality (44), then Eqs. (41b) and (41c) become

$$\theta_s^{(1-D)}(0,0,t)=\frac{\sqrt{\alpha}\Gamma_s}{k\sqrt{\pi}}\left\{\int_0^t\frac{q_0(t_0)}{(t-t_0)^{1/2}}\,dt_0 -\left(\frac{\pi}{\tau_h}\right)^{1/2}\int_0^t q_0(t_0)Y\left[\left(\frac{t-t_0}{\tau_h}\right)^{1/2}\right]dt_0\right\} \tag{45a}$$

and

$$\theta_b^{(1-D)}(0,0,t)=\frac{\alpha(1-\Gamma_s)}{k}\left(\int_0^t\frac{F(t_0)Y[\sqrt{(t-t_0)/\tau_h}]dt_0}{1-\sqrt{\tau_h/\tau_\beta(t_0)}} -\sqrt{\tau_h}\int_0^t\frac{F(t_0)Y[\sqrt{(t-t_0)/\tau_\beta}]dt_0}{\sqrt{\tau_\beta(t_0)}-\sqrt{\tau_h}}\right). \tag{45b}$$

In the special case of unsaturated laser media with ''instantaneous'' deexcitation time constant τ_{21} (i.e., when $\tau_{21}\simeq 0$ on the time scale of the earliest observation time t), the source term $F(t_0)$, Eq. (34b), can be written

$$F(t_0)=\frac{2I_0\beta_{30}}{\pi}\left(\frac{E_{30}^{\mathrm{NR}}}{E_{30}}\right)\begin{cases}1, & t_0<\tau_p,\\ 0, & t_0>\tau_p.\end{cases} \tag{46}$$

$q_0(t_0)$ is given by Eq. (36); $I_0\equiv P_o/R^2$ is the incident pump laser irradiance ($\mathrm{W/m^2}$). Inserting Eqs. (36) and (46) in Eqs. (45a) and (45b) with τ_β independent of time (completely unsaturated medium) and using the following easy-to-derive identities (T: any constant),

$$\int_0^t Y\left[\left(\frac{t-t_0}{T}\right)^{1/2}\right]dt_0=2\left(\frac{T}{\pi}\,t\right)^{1/2}-T\left[1-Y\left(\frac{t}{T}\right)^{1/2}\right] \tag{47}$$

and

$$\begin{aligned}\int_0^{\tau_p}&Y\left[\left(\frac{t-t_0}{T}\right)^{1/2}\right]dt_0\\ &=T\left\{Y\left[\left(\frac{t}{T}\right)^{1/2}\right]-Y\left[\left(\frac{t-\tau_p}{T}\right)^{1/2}\right]\right\}\\ &\quad+2\left(\frac{T}{\pi}\right)^{1/2}(\sqrt{t}-\sqrt{t-\tau_p}),\quad t\geqslant\tau_p,\end{aligned} \tag{48}$$

with the defined function

$$M(x)\equiv 1-\exp(x^2)\mathrm{erfc}(x) \tag{49}$$

as complementary to the function $Y(x)$, gives

$$\begin{aligned}\theta^{(1-D)}(0,0,t)&=\theta_s^{(1-D)}(0,0,t)+\theta_b^{(1-D)}(0,0,t)\\ &=\frac{2I_0}{\pi}\left(\frac{\sqrt{\alpha\tau_h}}{k}\right)\left\{\Gamma_s M\left(\frac{t}{\tau_h}\right)^{1/2}\right.\\ &\quad+\frac{(1-\Gamma_s)(E_{30}^{\mathrm{NR}}/E_{30})}{1-\sqrt{\tau_h/\tau_\beta}}\left[M\left(\frac{t}{\tau_\beta}\right)^{1/2}\right.\\ &\quad\left.\left.-\left(\frac{\tau_h}{\tau_\beta}\right)^{1/2}M\left(\frac{t}{\tau_h}\right)^{1/2}\right]\right\},\quad t\leqslant\tau_p\end{aligned} \tag{50a}$$

and

$$\theta^{(1-D)}(0,0,t)|_{t\geqslant\tau_p}=\theta^{(1-D)}(0,0,t)|_{t\leqslant\tau_p}-\theta^{(1-D)}(0,0,t-\tau_p)|_{t\leqslant\tau_p}. \tag{50b}$$

Further simplification occurs when the heat transfer coefficient is small, i.e., $\tau_h\gg t$. In this limiting adiabatic case, and with the further assumption $\tau_h\gg\tau_\beta$, expansion of erfc $(\sqrt{t/\tau_h})$ in a Taylor series around zero,[20] and use of the assumption of totally nonradiative deexcitation ($\eta_{\mathrm{NR}}=1\Rightarrow E_{30}^{\mathrm{NR}}=E_{30}$) yields

$$\begin{aligned}\theta^{(1-D)}(0,0,t)\simeq\frac{2I_0}{\pi}\left(\frac{\sqrt{\alpha}}{k}\right)&\left\{\Gamma_s\sqrt{\tau_h}M\left(\frac{t}{\tau_h}\right)^{1/2}\right.\\ &\left.+(1-\Gamma_s)\sqrt{\tau_\beta}\left[2\left(\frac{t}{\pi\tau_\beta}\right)^{1/2}-M\left(\frac{t}{\tau_\beta}\right)^{1/2}\right]\right\}.\end{aligned} \tag{51}$$

Equation (51) is a corrected form of the earlier result by Santos and Miranda, Ref. 2, Eqs. (26) and (27), in that the terms ''bulk'' and ''surface'' absorption (coefficients) in Ref. 2 must be replaced by $(1-\Gamma_s)$ and Γ_s, respectively. Here Γ_s represents surface absorptance,

$$\Gamma_s(\lambda)\equiv\beta_s(\lambda)l_s, \tag{52}$$

where $\beta_s(\lambda)$ is the surface absorption coefficient and l_s is the effective surface-layer thickness. The $\theta_b^{(1-D)}(0,0,t)$ part of Eq. (51) appears to have been first derived by Bechtel, with Γ_s having been replaced by the surface reflectance, R_s, in Bechtel's treatment, Ref. 6, Eq. (3.7). In the present theory, an additional factor $(1-R_s)$ should multiply all $\theta(0,0,t)$ expressions to account for Fresnel losses.

V. NUMERICAL SIMULATIONS OF $\theta(0,0,t)$ AND DISCUSSION

Several numerical simulations of the surface temperature as represented by Eqs. (41a)–(43b) have been implemented. Given our earlier applications to the Ti^{3+}:Al_2O_3 system, which was spectroscopically found to have separate contributions from bulk and surface absorptions,[11] various families of transient photothermal parametric responses were calculated using this laser material as the example. In addition, this material exhibits a saturation intensity value ($I_{\mathrm{sat}}\sim 2.6\times10^5\ \mathrm{W/cm^2}$)[21] experimentally attainable in photo-

thermal experiments under normal beam focusing conditions. With the exception of the parameter being varied to study the transient dependence on its assumed value(s), the rest of the parameters for a given photothermal response were set as follows[11] (default), unless stated otherwise: $\alpha=0.106$ cm^2/s; $K=33$ W/m K; $\eta_{\rm NR}$ (490 nm)$=0.1$; $P_o=6.0$ W; β_{30} (490 nm)$=1.0$ cm^{-1}; $W_{p0}=3\times10^4$ s^{-1}; $R=100$ μm; $\tau=3.18$ μs; $\tau_\beta=9.43$ s; $\tau_h=1$ ms; $\tau_{21}=3.5$ μs; and $\tau_p=3$ μs. The excited-state energetics used in the simulations were:[22] $E_{30}=19\,455$ cm^{-1}; $E_{32}=3239$ cm^{-1}; $E_{21}=14\,380$ cm^{-1}; $E_{10}=1836$ cm^{-1}, the same as in the simulations of Fig. 2. The main purpose of the simulations was the study of the relative strengths and temporal evolution profiles of the $\theta_s(0,0,t)$ and $\theta_b(0,0,t)$. The consideration of $\theta(0,0,t)$, instead of the experimentally more relevant average $(1/A)\int_0^A\Theta(r,0,t)r\,dr$, where A is the detector size, is meant to reflect the simplicity of the former representation, and the fact that it is a very good approximation of observed photothermal signals with infrared radiometric instrumentation,[3,8] in which the size of the HgCdTe detector ($\sim50\times50$ μm^2) is small compared to the pump laser beam radius ($\sim10^4$ μm^2). Appendix B gives the details of the numerical integration routines used with computer calculations.

The type of boundary condition describing heat loss from the surface of the optically heated medium affects greatly the transient decay profile. Within the linear approximation, the choice of a linear condition, Eq. (26e), is usually a popular one, since it encompasses the two extreme limits of isothermal ($h\rightarrow\infty$) and adiabatic ($h=0$) boundaries. Figure 4 shows the effect of the heat transfer rate on the bulk temperature component $\theta_b(0,0,t)$, Eqs. (42b), (43b) via the characteristic thermal transfer time τ_h, Eq. (31). Under three-dimensional (focused pump-beam) conditions, Fig. 4(a) shows that τ_h saturation occurs for $\tau_h\geqslant1$ s (adiabatic limit), while $\tau_h\leqslant1$ ms affects the decay curves on the $t<50$ μs time scale. Figure 4(b) indicates that, under one-dimensional conditions (unfocused pump laser beam), there is no decay of the photothermal bulk transient when $\tau_h\geqslant10^3$ s, due to fully adiabatic conditions and the loss of the lateral heat transfer pathways (or DOFs). These lateral energy DOFs are present with beam focusing and are responsible for the decaying behavior of the adiabatic curves ($\tau_h=1-10^3$ s) in Fig. 4(a). Furthermore, the signal intensity decreases dramatically when a constant-irradiance pump laser beam is spread from $R=100$ μm to 10^4 μm. This is not shown in the normalized plots of Figs. 4(a) and 4(b). Figure 5 shows the gradual transition from one- to three-dimensional configuration. For pump-beam waists $R\geqslant10^3$ μm one-dimensional behavior is observed, whereas the $R\leqslant10^2$ μm curves peak earlier, a clear indication that tight focusing interferes with the measurement of the relaxation time constant τ_{21}: The calculations show that it is necessary to know accurately the beam waist R for precise measurements of metastable state relaxation time constants, when $R^2/\alpha\sim200\tau_{21}$. In the situation shown in Fig. 5 knowledge of R becomes important for $R\leqslant100$ μm. Figure 6(a) shows that the effect of changing the value of τ_β on the evolution of the photothermal transient is similar to the effect of τ_h. Knowledge of τ_β [Eq. (A11)] is, however, much easier to obtain through spectroscopic and

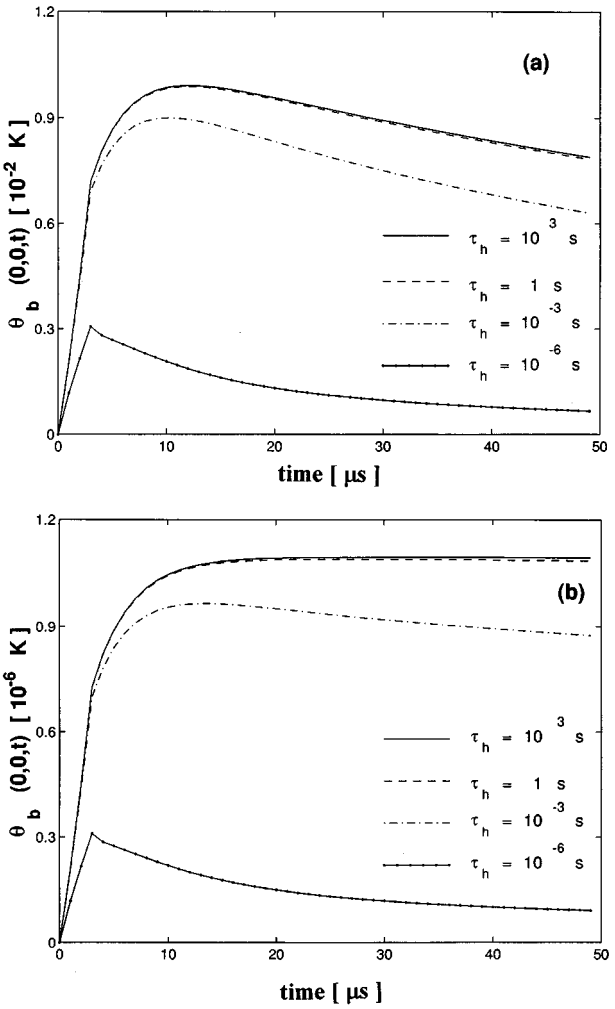

FIG. 4. $\theta_b(0,0,t)$ with a Gaussian pump laser beam of waist (a) 10^2 μm and (b) 10^4 μm as a function of τ_h. $\tau_p=3$ μs. Optical excitation of a Ti:sapphire rod was assumed at $\lambda=490$ nm where (Ref. 11) β_{30} (490 nm)$\simeq1$ cm^{-1} ($\tau_\beta=9.43$ s), and $\eta_{\rm NR}\simeq0.1$.

thermal measurements, and this parameter can be one of the inputs to theoretical modeling of experimental data from laser media. Figure 6(b) shows the effects of optical saturation, $\beta_{30}(t)$, on the photothermal transients for $\tau_\beta=10$ s; in Ti:sapphire τ_β ($\lambda=490$ nm)$\simeq9.43$ s. When optical saturation occurs due to intense irradiation, the resulting photothermal signal, Eqs. (42b) and (43b), decreases in comparison with the fully unsaturated transient, owing to the decrease in $\beta_{30}(t)$, Eq. (18).

In order to understand the dependence of the $\theta_b(0,0,t)$ on the dynamic parameters of the metastable state $|2\rangle$ it is instructive to study the profile of the bulk thermal source, i.e., the evolution of the heating (nonradiative) rate density $dQ(t)/dt$, Eq. (19); Fig. 2 shows this function, which is also identical (up to a constant term) to $F(t)$, Eq. (34b). The asymmetry in the rise and decay times is due to the dependence of τ on W_{p0}, Eq. (9), when the pumping rate $W_{p0}\geqslant10^4$ s^{-1}. High pump rates of the excited state result in earlier saturation (flattening) of the thermal flux per unit depth released in the bulk of the laser medium, due to the high transition rate out of the ground state and attainment of

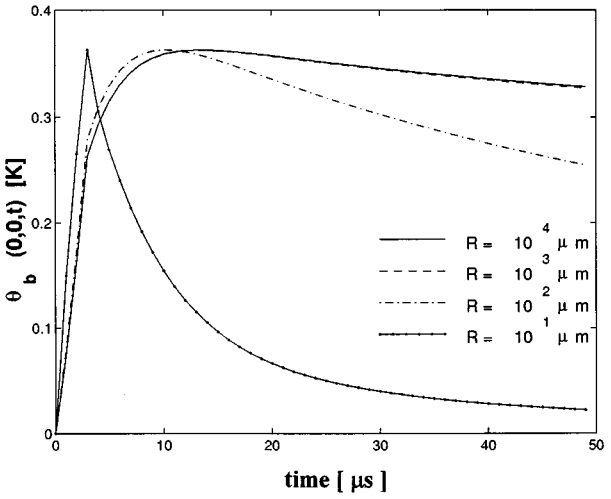

FIG. 5. $\theta_b(0,0,t)$ with a Gaussian pump laser beam and its beam waist as a parameter. $\tau_p=3$ μs; $\tau_h=1$ ms ($h=3.2\times10^4$ W/m^2 K). Profiles are normalized to the maximum value for $R=10$ μm.

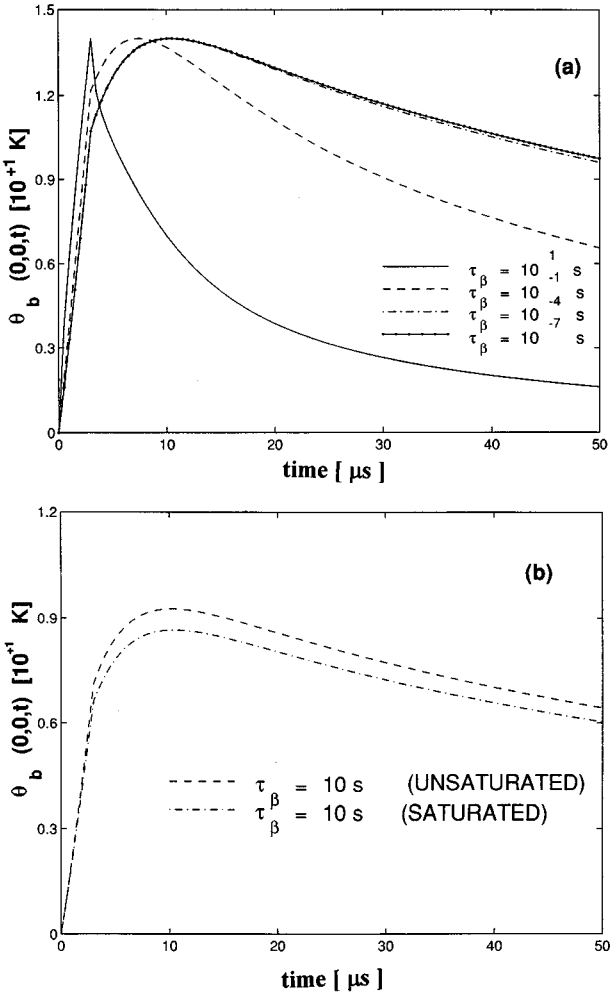

FIG. 6. (a) $\theta_b(0,0,t)$ with τ_β as a parameter. (b) Comparison of $\theta_b(0,0,t)$ profile for a saturated and on unsaturated laser medium. τ_β corresponds to the maximum absorption coefficient, in the β_m saturated case. In the fully unsaturated case $\tau_\beta=(\beta_m^2\alpha)^{-1}$.

the maximum dynamic steady-state population inversion of the metastable laser level $|2\rangle$. Once saturation (i.e., dynamic steady state) has been attained and the optical pump is switched off, nonradiative decay controlled by the lifetime τ_{21} takes place, irrespective of the rate at which the dynamic steady state was attained, Fig. 2. Upon letting $\tau_{21}=0$, both thermal buildup and decay become instantaneous, the former leading to $\tau=0$, Eq. (9), independent of W_{p0}. In this limiting case the simple photothermal source profile of a rectangular (time-gated) pulse ensues. It should be noted that the transient time constants governing the evolution of Fig. 2 are the same as those governing the evolution of the level $|2\rangle$ population $N_2(t)$, Eq. (18). Therefore, it has been found to be more convenient to monitor the luminescence transient experimentally and deduce from the rise and decay times the time constants τ_{21} and τ.[23] This combined luminescence-photothermal approach offers the advantage of a simple integrated experimental setup with the superior SNR of the luminescence transient, the results of which can be used as input data to the photothermal signal modeling. Figure 7 shows theoretical luminescence transients, Eq. (8), corresponding to the thermal rate density curves of Fig. 2.

When the profiles of Fig. 2 are used with Eqs. (42b) and (43b) with τ_{21} as a parameter, the results are the photothermal transients shown in Fig. 8 proceeding from the instantaneous deexcitation, $\tau_{21}=0$, case to $\tau_{21}>1$ μs. The expected shift of the time-delay maximum from $t-\tau_p=0$ to progressively later times is clearly observed, along with a delay in the rise time due to the delayed heat release from level $|2\rangle$. There is, of course, the nonradiative transition from level $|3\rangle$ to level $|2\rangle$ which is instantaneous on the μs observation time scale. The heat release from this source is responsible for the $\theta_b(0,0,t)$ rise from the background (zero) level immediately upon the onset of the optical pulse. As discussed in Sec. II, once all thermal energy is released from level $|2\rangle$, another (instantaneous) nonradiative decay occurs from level $|1\rangle$ to the ground state $|0\rangle$ and further thermal evolution is governed by conduction in the Ti:sapphire rod. Therefore, all transients assume identical decay shapes at times $t\gg\tau_{21}$, Fig. 8.

The final sets of numerical simulations were aimed at assessing the relative strength of bulk and surface absorptance nonradiative sources. The important surface absorptance parameter Γ_s (490 nm) was used as a variable parameter to investigate surface-layer-induced temperature transients $\theta_s(0,0,t)$, Eq. (41b). Based on the earlier spectroscopic results with polished Ti:sapphire rods,[11] transients in the $0.01\leqslant\Gamma_s$ (490 nm)$\leqslant0.2$ range were investigated. The 100% nonradiative nature of the surface-layer deexcitation following a rectangular optical pulse shows instantaneous relaxation profiles similar to those obtained experimentally with opaque samples.[24] Figure 9(a) compares the strengths of $\theta_b(0,0,t)$ and $\theta_s(0,0,t)$ in forming the temperature envelope $\theta(0,0,t)$. The results show that the surface term in the $\theta(0,0,t)$ distribution, Eq. (41b), can easily be dominant, especially in the range Γ_s (490 nm)$\simeq0.1$.[11] At best, the relative signal strengths can become similar only at times much longer than τ_p, typically for $t>3$ ms, Fig. 9(b), for the laser rod with the default parameters of Fig. 9(a). The crossover in Fig. 9(b) occurs as delayed heat arrives at the rapidly cooled surface from deep regions in the bulk at times much longer

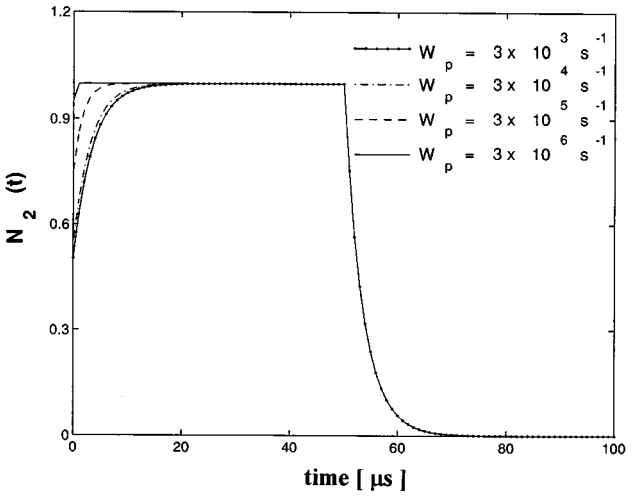

FIG. 7. $N_2(t)$ profiles, Eq. (8), corresponding to the $dQ(t)/dt$ profiles in Fig. 2.

than the surface cooling time $\tau_h = 1$ ms. This effect indicates that photothermal characterization of the bulk or the surface can be carried out successfully via time-gating of the transient response to a laser source at long or short times, respectively, following the pulse cutoff. An ideal scheme for this type of detection is the photothermal RW technique[3] which offers temporal sample response discrimination through scanning of the duration τ_p of a time-gated square laser pulse.[25] Therefore, it can be concluded that photothermal techniques can be used efficiently to measure the effect of surface damage, such as polishing procedures, in laser media, specifically as nonradiative surface layers (NRSLs),[11] or as deexcitation sites: Figure 9 indicates that the nonradiative state of the laser rod surface must be carefully assessed and optimized by minimizing $\Gamma_s(\lambda)$, since nonoptimal surface polishes or other damage in the form of NRSLs may in fact negate any benefits of low bulk nonradiative deexcitation site/defect densities. Regarding the extent to which the nonradiative quantum yield η_{NR} of the level $|2\rangle$ affects the evolution of the photothermal signal, although a straightforward matter in the theoretical formalism, yet it may be quite hard to deconvolve experimentally the η_{NR} contribution alone from the photothermal transients, unless all other parameters are accurately known. From the results of Fig. 9(a) it appears that a static spectroscopic determination of $\eta_{\mathrm{NR}}(\lambda)$ using frequency-domain quadrature-photopyroelectric detection[11] may be preferable to the time-domain method.

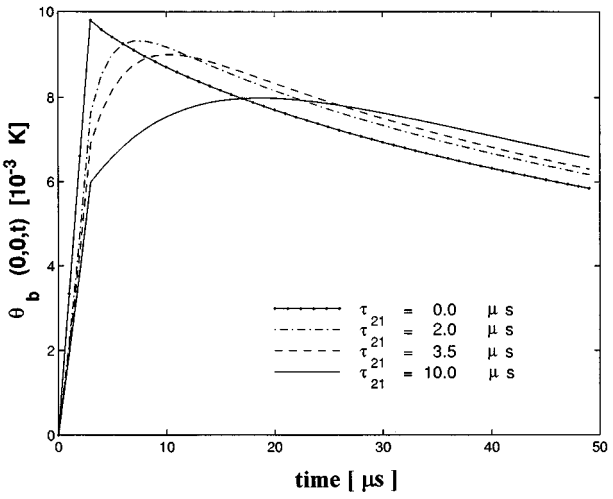

FIG. 8. $\theta_b(0,0,t)$ with τ_{21}, as a parameter.

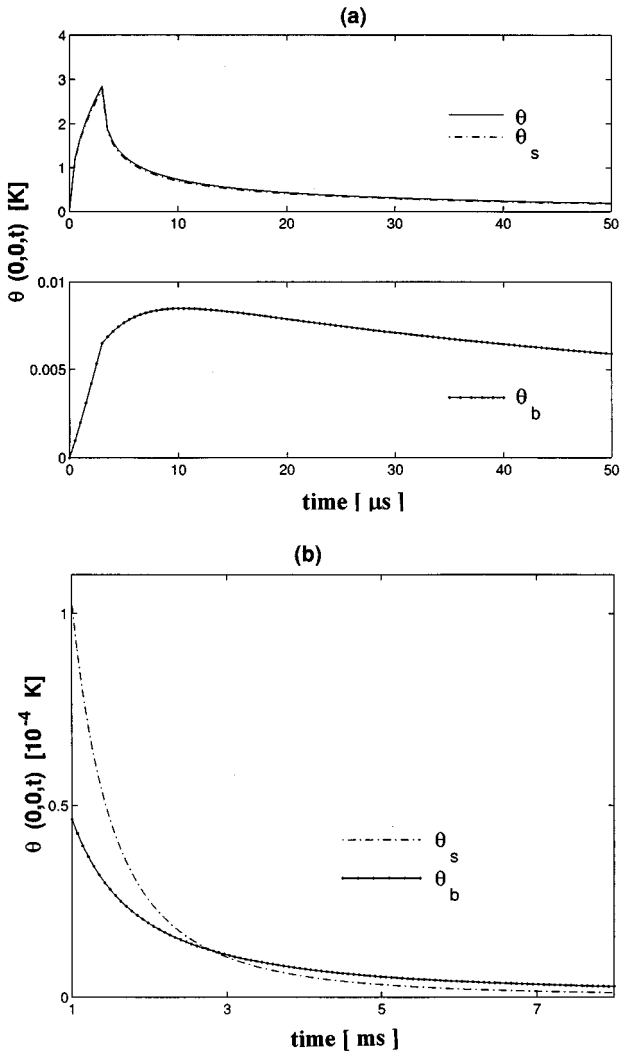

FIG. 9. $\theta(0,0,t)$ and separate $\theta_b(0,0,t)$ and $\theta_s(0,0,t)$ profiles for $\Gamma_s = 0.02$: (a) short time; and (b) long-time relaxation scales and signal crossover.

VI. CONCLUSIONS

A rigorous theoretical treatment of the optical and photothermal transient evolution from solid-state laser media excited by intense focused laser irradiation was presented. Both surface and bulk sources were considered. Explicit field functions were derived for the surface temperature transients including saturation, and applications to the Ti^{3+}:Al_2O_3 laser rod system were simulated. The major results of these numerical simulations were

(i) the sensitivity of the photothermal signal to the presence of small (nonzero) surface absorptions, espe-

cially the tendency of the surface nonradiative centers to dominate the bulk photothermal signal via their very efficient (100%) optical-to-thermal energy conversion;

(ii) the distinctly different thermal profiles obtained from bulk and from surface nonradiative deexcitations;

(iii) the advantage of monitoring the luminescence signal transient of the laser medium in order to obtain important information on the spontaneous lifetime and optical pumping rate of the medium; and

(iv) the complementarity of luminescence and photothermal transient profiles.

The theory developed in this work points to the sensitivity of photothermal techniques to the highly efficient nonradiative (optical-to-thermal) energy conversion processes at the laser rod surface. This, in turn, suggests the so far little noticed practical importance of optimizing the usual surface polishes of laser rods, in order to minimize the NRSLs which arise from residual damage due to this procedure. The present analysis shows that photothermal detection can offer an otherwise very difficult measure of assessing the nonradiative efficiency of surface layers in solid-state laser media as serious limiters of the figure of merit in manufactured laser rods.

The theory is currently being applied to the modeling of infrared photothermal radiometric experimental data from Ti:sapphire crystal rods in our laboratory.

ACKNOWLEDGMENT

The authors wish to gratefully acknowledge a Research Grant from the Natural Sciences and Engineering Research Council of Canada (NSERC), which made this work possible.

APPENDIX A

Analytical calculation of $K(r,t;t_0)$, Eq. (38)

Using the definition of the integral K and the radial Green's function, Eq. (28),

$$K(r,t;t_0)=\frac{1}{4\pi\alpha(t-t_0)}\exp\left(-\frac{r^2}{4\alpha(t-t_0)}\right)\times\int_0^\infty\exp\left[-\left(\frac{1}{4\alpha(t-t_0)}+\frac{2}{R^2}\right)r_0^2\right]\times I_o\left(\frac{rr_0}{2\alpha(t-t_0)}\right)r_0\,dr_0. \tag{A1}$$

From Ref. 26, entry 6.633.4, p. 718, one obtains

$$\int_0^\infty e^{-ax^2}I_\nu(\beta x)J_\nu(\gamma x)x\,dx=\frac{1}{2a}\exp\left(\frac{\beta^2-\gamma^2}{4a}\right)J_\nu\left(\frac{\beta\gamma}{2a}\right). \tag{A2}$$

Letting

$$a\equiv\frac{1}{4\alpha(t-t_0)}+\frac{2}{R^2},\quad \nu=0,\quad \beta\equiv\frac{r}{2\alpha(t-t_0)},\quad \gamma=0,$$

gives upon algebraic manipulation an explicit representation for the integral in Eq. (A1),

$$K(r,t;t_0)=\frac{R^2}{2\pi[8\alpha(t-t_0)+R^2]}\times\exp\left(-\frac{2r^2}{8\alpha(t-t_0)+R^2}\right). \tag{A3}$$

Analytical calculation of $H(t;t_0)$, Eq. (39)

Using the definition of the integral H and the axial Green's function, Eq. (29),

$$H(t;t_0)=\frac{2}{\sqrt{4\pi\alpha(t-t_0)}}\int_0^\infty\exp\left[-\left(\frac{z_0^2}{4\alpha(t-t_0)}+\beta_{30}(t_0)z_0\right)\right]dz_0-\frac{1}{\sqrt{\alpha\tau_h}}\exp\left(\frac{t-t_0}{\tau_h}\right)\times\int_0^\infty\exp\left[\left(\frac{1}{\sqrt{\alpha\tau_h}}-\beta_{30}(t_0)\right)z_0\right]\times\operatorname{erfc}\left[\frac{z_0}{\sqrt{4\alpha(t-t_0)}}+\left(\frac{t-t_0}{\tau_h}\right)^{1/2}\right]dz_0. \tag{A4}$$

From Ref. 26, entry 3.322.2, p. 307, the first integral gives

$$\int_0^\infty\exp\left[-\left(\frac{z_0^2}{4\alpha(t-t_0)}+\beta_{30}(t_0)z_0\right)\right]dz_0=\sqrt{\pi\alpha(t-t_0)}\,Y[\beta_{30}(t_0)\sqrt{\alpha(t-t_0)}], \tag{A5}$$

where the function $Y(z)$ was defined in Eq. (30) and $\beta_{30}(t)$ was defined in Eq. (18). For the second integral in Eq. (A4), let

$$J\equiv\int_0^\infty\exp\left[\left(\frac{1}{\sqrt{\alpha\tau_h}}-\beta_{30}(t_0)\right)z_0\right]\times\operatorname{erfc}\left[\frac{z_0}{\sqrt{4\alpha(t-t_0)}}+\left(\frac{t-t_0}{\tau_h}\right)^{1/2}\right]dz_0. \tag{A6}$$

An integration by parts, using the definition

$$\operatorname{erfc}(x)=\frac{2}{\sqrt{\pi}}\int_x^\infty e^{-y^2}\,dy \tag{A7}$$

gives

$$J=\left(\frac{1}{\sqrt{\alpha\tau_h}}-\beta_{30}(t_0)\right)^{-1}\left\{\frac{1}{\sqrt{\pi\alpha(t-t_0)}}\exp\left[-\left(\frac{t-t_0}{\tau_h}\right)\right]\times\int_0^\infty\exp\left[-\left(\frac{z_0^2}{4\alpha(t-t_0)}+\beta_{30}(t_0)z_0\right)\right]dz_0-\operatorname{erfc}\left(\frac{(t-t_0)}{\tau_h}\right)^{1/2}\right\}. \tag{A8}$$

Inserting Eq. (A5) in the integral on the right-hand side of Eq. (A8) yields

$$J=\left(\frac{1}{\sqrt{\alpha\tau_h}}-\beta_{30}(t_0)\right)^{-1}\left\{\exp\left[-\left(\frac{t-t_0}{\tau_h}\right)\right]\right.$$
$$\left.\times Y[\beta_{30}(t_0)\sqrt{\alpha(t-t_0)}]-\operatorname{erfc}\left[\left(\frac{t-t_0}{\tau_h}\right)^{1/2}\right]\right\}. \quad \text{(A9)}$$

Finally, returning to Eq. (A4) and inserting the analytical expressions (A5) and (A9) gives the following result for H:

$$H(t;t_0)=\frac{1}{1-\sqrt{\tau_h/\tau_\beta(t_0)}}\left\{Y\left[\left(\frac{t-t_0}{\tau_h}\right)^{1/2}\right]\right.$$
$$\left.-\left(\frac{\tau_h}{\tau_\beta(t_0)}\right)^{1/2}Y\left[\left(\frac{t-t_0}{\tau_\beta(t_0)}\right)^{1/2}\right]\right\}, \quad \text{(A10)}$$

where the definition

$$\tau_\beta(t_0)\equiv[\beta_{30}^2(t_0)\alpha]^{-1} \quad \text{(A11)}$$

was made,[27] to indicate the photothermal transit time (including optical saturation) of heat generated within one optical absorption length, β_{30}^{-1}, from the surface of a laser medium with thermal diffusivity α.

APPENDIX B: NUMERICAL INTEGRATION ALGORITHMS FOR EQS. (41a)–(43b)

In the computation of $Y(z)=\exp(z^2)\operatorname{erfc}(z)$, the complementary error function was considered as a special case of the incomplete gamma function,

$$\Gamma(a,z)=\frac{1}{\Gamma(a)}\int_z^\infty e^{-t}t^{a-1}\,dt, \quad \text{(B1)}$$

through the relation[28]

$$\operatorname{erfc}(z)=1-\Gamma(1/2,z^2). \quad \text{(B2)}$$

Using the representation of the incomplete gamma function in terms of continued fractions, Ref. 29, entry 6.5.31,

$$\Gamma(a,z)=e^{-z}z^a\left(\frac{1}{z+}\,\frac{1-a}{1+}\,\frac{1}{z+}\,\frac{2-a}{1+}\,\frac{2}{z+}\cdots\right), \quad z>0, \quad \text{(B3)}$$

gives the following expression:

$$\operatorname{erfc}(z)=t\,\exp[-z^2-1.265\,512\,23+t(1.000\,023\,68+t(0.374\,091\,96+t(0.096\,784\,18+t(-0.186\,288\,06+t(0.278\,868\,07$$
$$+t(-1.135\,203\,98+t(1.488\,515\,87+t(-0.822\,152\,23+(0.170\,872\,77t)))))))))], \quad \text{(B4a)}$$

where

$$t=(1+0.5z)^{-1}. \quad \text{(B4b)}$$

Equation (B4) was found to be a very accurate representation of $\operatorname{erfc}(z)$, up to $O(10^{-8})$, and was used in all further integration routines.

Computations of the required integrals were performed using Romberg integration on an open interval.[30] This procedure returns the integral of a function with given end points using the extended midpoint rule. According to this rule, an estimate of $\int_a^b f(x)dx$ will be returned when it is first called $(n=1)$. Subsequent refinements $(n=2,3,4,\ldots)$ will improve the accuracy of the return variable by adding $(2/3)\times 3^{n-1}$ additional interior points. In other words, the foregoing procedure computes the nth stage of refinement of the extended midpoint rule.

[1] A. Mandelis and B. S. H. Royce, J. Appl. Phys. **51**, 610 (1980).
[2] R. Santos and L. C. M. Miranda, J. Appl. Phys. **52**, 4194 (1981).
[3] A. Mandelis, Z-H. Chen, and R. Bleiss, Opt. Eng. (Bellingham) **32**, 2046 (1993).
[4] A. M. Buoncristiani, C. E. Byvik, and U. O. Farrukh, Proc. SPIE **892**, 68 (1988).
[5] J. D. Foster and L. M. Osterink, J. Appl. Phys. **41**, 3656 (1970).
[6] J. H. Bechtel, J. Appl. Phys. **46**, 1585 (1975).
[7] W. Koechner, J. Appl. Phys. **44**, 3162 (1973).
[8] A. Mandelis, M. Munidasa, and A. Othonos, IEEE J. Quantum Electron. **QE-29**, 1498 (1993).
[9] A. Mandelis, J. Vanniasinkam, S. Buddhudu, A. Othonos, and M. Kokta, Phys. Rev. B **48**, 6808 (1993II).
[10] W. R. Rapoport and C. P. Khattak, Appl. Opt. **27**, 2677 (1988).
[11] J. Vanniasinkam, A. Mandelis, S. Buddhudu, and M. Kokta, J. Appl. Phys. **75**, 8090 (1994).
[12] O. Svelto, *Principles of Lasers*, 3rd ed., transl. by D. C. Hanna (Plenum, New York, 1993).
[13] M. Grinberg, A. Mandelis, and K. Fjeldsted, Phys. Rev. B **48**, 5935 (1993).
[14] P. Albers, E. Stark, and G. Huber, J. Opt. Soc. Am. B **3**, 134 (1986).
[15] M. Grinberg and A. Mandelis, Phys. Rev. B **49**, 12 496 (1994II).
[16] M. N. Ozisik, *Boundary Value Problems of Heat Conduction* (Dover, New York, 1968).
[17] P. L. Chambré, J. Appl. Phys. **30**, 1683 (1959).
[18] J. V. Beck, K. D. Cole, A. Haji-Sheikh, and B. Litkouhi, *Heat Conduction using Green's Functions* (Hemisphere, Washington, DC, 1992).
[19] A. Mandelis and J. F. Power, Appl. Opt. **27**, 3397 (1988).
[20] H. S. Carslaw and J. C. Jaeger, *Conduction of Heat in Solids* (Oxford University Press, Oxford, 1959), Appendix II.
[21] J. F. Pinto, L. Esterowitz, G. H. Rosenblatt, M. Kokta, and D. Peressini, IEEE J. Quantum Electron. **QE-30**, 2612 (1994).
[22] B. F. Gachter and J. A. Koningstein, J. Chem. Phys. **60**, 2003 (1974).
[23] J. Vanniasinkam and A. Mandelis (unpublished).
[24] D. L. Balageas, J. C. Krapez, and P. Cielo, J. Appl. Phys. **59**, 348 (1986).
[25] M. Munidasa and A. Mandelis, Rev. Sci. Instrum. **65**, 2344 (1994).
[26] I. S. Gradshteyn and I. M. Ryzhik, *Table of Integrals, Series and Products* (Academic, Orlando, 1980).
[27] A. Mandelis and B. S. H. Royce, J. Appl. Phys. **50**, 4330 (1979).
[28] E. Jahnke and F. Emde, *Tables of Functions with Formulae and Curves*, 4th ed. (Dover, New York, 1945), p. 23.
[29] M. Abramowitz and I. A. Stegun, *Handbook of Mathematical Functions*, Appl. Math. Series, Vol. 55 (NBS, Washington, DC, 1964).
[30] W. H. Press, S. A. Teukolsky, W. T. Vetterling, and B. P. Flannery, *Numerical Recipes* (Cambridge University Press, Cambridge, 1992).